DOI: 10.1002/chem.200902005

A Selective, Nontoxic, OFF–ON Fluorescent Molecular Sensor Based on 8-Hydroxyquinoline for Probing Cd^{2+} in Living Cells

Marta Mameli,[a] M. Carla Aragoni,[a] Massimiliano Arca,[a] Claudia Caltagirone,[a] Francesco Demartin,[b] Giovanna Farruggia,[c] Greta De Filippo,[a] Francesco A. Devillanova,[a] Alessandra Garau,[a] Francesco Isaia,[a] Vito Lippolis,*[a] Sergio Murgia,[d] Luca Prodi,[e] Anna Pintus,[a] and Nelsi Zaccheroni[e]

Abstract: In spite of the fact that cadmium(II) has been recognized as a highly toxic element and that excessive exposure to this metal ion has been reported to have many adverse effects on human health, very few selective and specific fluorescent probes are available for imaging Cd^{2+} in living cells. Herein, we report the spectroscopic and photochemical characterization of 5-(5-chloro-8-hydroxyquinolinylmethyl)-2,8-dithia-5-aza-2,6-pyridinophane (**L**) as a fluorescent sensor for the selective imaging of Cd^{2+} in living cells. In particular, the response of **L** to Cd^{2+} was first assessed in aqueous solutions, sodium dodecyl sulfate micelles, and liposomes, and subsequently in living cells by fluorescence microscopy techniques. Cytofluorimetric analyses of leukemic HL-60 cells loaded with **L** also allowed evaluation of the toxicity of the probe and the selective analysis of its intracellular fluorescence in the presence of Cd^{2+}. Furthermore, the 1:1 complex species $[Cd(\mathbf{L})H_2O]^{2+}$ responsible for the OFF–ON chelation enhancement of fluorescence (CHEF) effect on **L** was structurally characterized; time-dependent DFT calculations allowed the prediction of theoretical excitations, which were comparable with the experimental ones.

Keywords: cadmium · density functional calculations · fluorescent probes · imaging agents · macrocycles

Introduction

Few metals in their ionic state are essential to plant and animal life. Four of these (Na, K, Mg, and Ca) are present in large quantities; the others, present in small quantities, are d-block elements and can be divided into two subgroups: trace metals (Fe, Cu, and Zn) and ultratrace metals (Co, Mo, Cr, V, Mn, and Ni). Their role is either structural (they help to stabilize certain protein structures) or functional (they are involved in the reactivity of biosites).[1,2] The pathological alteration of the optimal required quantity of these metals in living cells is the cause and/or effect of important metabolic disorders.[3,4] Another crucial aspect is that living organisms can easily absorb and accumulate from the environment other metals that are not necessary for their survival (and therefore toxic, for example, Hg, Pb, Cd), thus causing dangerous conditions of intoxication and adverse effects upon human health.[3,4] With the possible exceptions of acute iron toxicity from intentional or unintentional ingestion and suspected lead exposure, emergency physicians will rarely be alerted to the possibility of metal exposure. Therefore, there is a great need for reliable, selective, and sensitive probes and methods for detecting and monitoring metal levels (including the highly toxic ones) in

[a] M. Mameli, Dr. M. C. Aragoni, Dr. M. Arca, Dr. C. Caltagirone, G. De Filippo, Prof. F. A. Devillanova, Dr. A. Garau, Prof. F. Isaia, Prof. Dr. V. Lippolis, A. Pintus
Dipartimento di Chimica Inorganica ed Analitica
S.S. 554 Bivio per Sestu
Università degli Studi di Cagliari
09042 Monserrato, CA (Italy)
Fax: (+39) 070-675-4456
E-mail: lippolis@unica.it

[b] Prof. F. Demartin
Dipartimento di Chimica Strutturale e Stereochimica Inorganica
Università di Milano
Via G. Venezian 21, 20133 Milano (Italy)

[c] Dr. G. Farruggia
Dipartimento di Biochimica "G. Moruzzi"
Università degli Studi di Bologna
Via S. Donato 19/2, 40127 Bologna (Italy)

[d] Dr. S. Murgia
Dipartimento di Scienze Chimiche, S.S. 554 Bivio per Sestu
Università degli Studi di Cagliari
09042 Monserrato, CA (Italy)

[e] Prof. Dr. L. Prodi, Dr. N. Zaccheroni
Dipartimento di Chimica "G. Ciamician"
Università degli Studi di Bologna
Via Selmi 2, 40126 Bologna (Italy)

Supporting information for this article is available on the WWW under http://dx.doi.org/10.1002/chem.200902005.

living cells and tissue samples. The development of these probes is of great importance to understand in detail the intracellular equilibria and mechanisms of distribution, to localize the cellular subcompartments of accumulation in the case of poisoning and metabolic disorder, and thus to diagnose pathological conditions in real time.[5,6]

Sensitive and reliable fluorescent molecular sensors seem to be the ideal tool for evaluating and dynamically mapping the intracellular fluctuations of metal ions by using microscopy techniques to allow real-time local imaging.[7–17] Besides selectivity/specificity and sensitivity properties, fluorescent molecular sensors for in vivo metal-ion mapping must also be able to operate in aqueous media, penetrate cell membranes, and change their fluorescence emission at physiological pH by interacting selectively with the targeted metal ions. Another parameter to consider for in vivo metal-ion mapping is also the excitation wavelength of the fluorescent probe, which should be as long as possible (near-infrared (NIR) or visible) in order not to damage tissues, cells, or their subcomponents that generally absorb short-wavelength radiations and could also filter them significantly. For many applications, however, it is not strictly necessary to perform in vivo analysis but the detection of these metals in vitro in tissues, living cells, or fixed ones can be more suitable. Therefore, selective and sensitive probes for in vitro measurements, which should have much fewer requirements and restrictions, are equally valuable. Their intrinsic toxicity and the damage caused by possible high-energy excitation by light (depending on the nature of the fluorogenic fragment in the sensor), for example, need to be low enough to ensure the survival of the cells for the time of the measurements and not be influential in the case of fixed cells.

Up to now, there have been only a few reports on the imaging of the toxic Hg^{2+},[12,13] Pb^{2+},[14] and Cd^{2+}[15–17] ions in living cells by using fluorescent chemosensors. In particular, cadmium is currently used in many industrial processes and the resulting high level of contamination in soil, water, and food is raising great concern.[18,19] This element is inessential for life and listed by the U.S. Environmental Protection Agency as one of 126 priority pollutants. Its half-life in humans is estimated to be between 15 and 20 years, and excessive exposure to it is reported to have toxic effects on procreation, bones, kidney, and nerve systems, thus resulting in renal dysfunction and calcium metabolism disorders, and pulmonary, prostatic, and renal cancer.[18,20,21] Therefore, there is a great need for fluorescent chemosensors for monitoring cadmium levels in living cells or tissue samples. The main challenge in the design of selective fluorescent molecular sensors for in vivo mapping of Cd^{2+} is to find systems that can discriminate Cd^{2+} from the ubiquitous Zn^{2+} under physiological conditions, the latter being normally present in cells and at relatively high concentrations.[22–24] The chemical behavior of these two metal ions is very similar due to their electronic closed-shell d^{10} configuration, and, therefore, they usually cause similar spectral changes after interactions with fluorescent sensors.

In the last few years, fluorescent chemosensors featuring 8-hydroxyquinoline (8-HDQ) derivatives as fluorogenic fragments have proved to be very effective in selectively discriminating Cd^{2+} over Zn^{2+} in solution, or Mg^{2+} over Ca^{2+} in solution and living cells.[7,25a–c] Recently,[25d] we also reported on the synthesis, basic coordination properties, and optical response to a series of "borderline" and "soft" metal ions in MeCN/H_2O mixtures, for a new class of fluorescent chemosensors based on the N_2S_2-donating 12-membered macrocycle 2,8-dithia-5-aza-2,6-pyridinophane appended with different fluorogenic groups. In particular, the derivative **L**, which bears a 5-chloro-8-hydroxyquinolinylmethyl pendant arm, demonstrated a selective chelation enhancement of fluorescence (CHEF)-type OFF–ON response to the presence of Cd^{2+} that was about four times higher than that to the presence of Zn^{2+} in MeCN/H_2O (1:1 v/v) solutions.

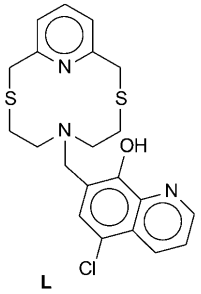

L

Herein, we report the structural and physical–chemical properties of the complex species $[Cd(\mathbf{L})H_2O]^{2+}$ responsible for the OFF–ON selective CHEF effect on **L**, and we investigate **L** as a fluorescent chemosensor for Cd^{2+} in aqueous solutions, sodium dodecyl sulfate (SDS) micelles, liposomes, and living cells. We also explore, through fluorescence techniques, the selectivity/specificity and spectroscopic response of the system to Cd^{2+} complexation in these media.

Results and Discussion

Characterization of the 1:1 complex between Cd^{2+} and L: X-ray crystal structure and DFT calculations: Previously, we studied the Cd^{2+}/**L** system potentiometrically in MeCN/H_2O (1:1 v/v) at 25 °C.[25d] Formation of the complex species $[Cd(\mathbf{L})]^{2+}$ was observed. It proved to be responsible for the selective CHEF effect recorded at neutral pH on addition of Cd^{2+} to MeCN/H_2O (1:1 v/v) solutions of **L**. The well-known high tendency of 8-HDQ derivatives to bind metal ions in their deprotonated form suggested that in $[Cd(\mathbf{L})]^{2+}$ the metal center could be coordinated to the deprotonated 5-Cl-8-HDQ unit of **L**,[25d] an acidic proton being localized either on the amine group of the macrocyclic moiety or on the nitrogen donor of the 5-Cl-8-HDQ framework. After many attempts, we succeeded in growing orange single crystals of the $[Cd(\mathbf{L})H_2O](ClO_4)_2$·MeCN complex suitable for X-ray diffraction analysis, from the complexation reaction of **L** with $Cd(ClO_4)_2$·$6H_2O$ in MeCN, followed by diffusion of Et_2O vapor into the reaction mixture. In this complex, an overall distorted octahedral geometry is reached at the metal center. One of the two mutually *cis* positions left free by the N_2S_2-donor set of the macrocyclic framework is occupied by the deprotonated hydroxyl group of the 5-Cl-8-

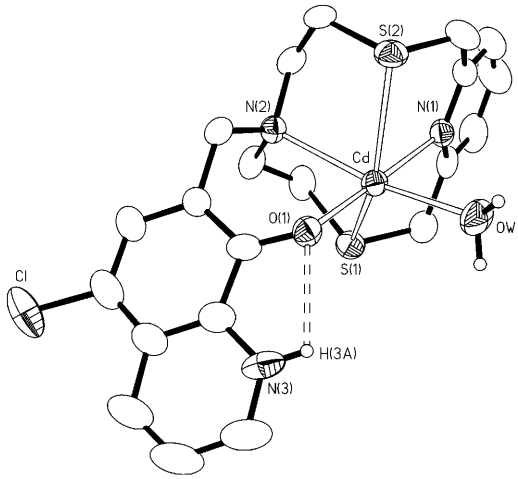

Figure 1. ORTEP view of the complex cation $[Cd(\mathbf{L})H_2O]^{2+}$ in $[Cd(\mathbf{L})H_2O](ClO_4)_2$·MeCN with the adopted labeling scheme. Displacement ellipsoids are drawn at a 30% probability level. Counter anions and hydrogen atoms, except that on N(3) and those belonging to the coordinated water molecule, have been omitted for clarity. Cd–N(1) 2.3886(19), Cd–N(2) 2.4545(18), Cd–S(1) 2.6354(9), Cd–S(2) 2.6351(8), Cd–O(1) 2.1810(15), Cd–Ow 2.3108(17) Å; N(1)-Cd-N(2) 94.40(6), N(1)-Cd-S(1) 75.43(5), N(1)-Cd-S(2) 76.81(5), N(1)-Cd-O(1) 178.81(6), N(1)-Cd-Ow 87.93(6), N(2)-Cd-S(1) 77.91(4), N(2)-Cd-S(2) 78.32(4), N(2)-Cd-O(1) 85.57(5), N(2)-Cd-Ow 166.98(6), S(1)-Cd-S(2) 141.60(2), S(1)-Cd-O(1) 105.71(5), S(1)-Cd-Ow 115.03(4), S(2)-Cd-O(1) 102.02(5), S(2)-Cd-Ow 89.78(5), O(1)-Cd-Ow 91.85(6)°.

HDQ unit; the other is occupied by a coordinated water molecule (Figure 1). The nitrogen atom of the fluorogenic framework is protonated to give an $NH^{+}\cdots O^{-}$ [N(3)H(3A)···O(1) 2.291(2) Å, N(3)···O(1) 2.650(3) Å, N(3)-H(3A)···O(1) 105.2(1)°) hydrogen bond with the adjacent deprotonated oxygen atom of the same 5-Cl-8-HDQ moiety. Therefore, upon complexation a proton is transferred from the hydroxyl group to the aromatic nitrogen atom within the 5-Cl-8-HDQ unit of **L**. To the best of our knowledge, this is only the third structure reported so far of a transition-metal complex featuring an 8-HDQ moiety coordinating in a zwitterionic form via the deprotonated hydroxyl function.[26] In $[Cd(\mathbf{L})H_2O]^{2+}$ the macrocyclic framework of **L** adopts the usual folded conformation resembling an open book with the spine along the S(1)-Cd-S(2) direction and the N(1)-Cd-N(2) hinge angle of 94.40(6)°. The plane containing the 5-Cl-8HDQ moiety is tilted by 39° with respect to the pseudo-plane defined by the metal center and the N(1), N(2), O(1), and water oxygen (Ow) atoms.

A density functional theoretical investigation[27] was undertaken to obtain an insight into the structural and chemical–physical features of the cationic complex $[Cd(\mathbf{L})H_2O]^{2+}$ (see Experimental Section). Ground-state geometry optimization was performed starting from structural data, and hypothesizing that either the N(3) or O(1) atoms could be protonated. A comparison of the total electronic energies showed that, neglecting solvation effects, the N(3)-protonated isomer (optimized N(3)–H(3A) distance 1.025 Å) is more stable by about 12 kcal mol^{-1} than the O(1)-protonated one, in agreement with experimental structural evidence. A comparison of experimental and calculated bond lengths and angles shows that all of the optimized values are very close to the corresponding experimental ones (see Figure 1 caption).[28] The natural bond orbital (NBO) charge distribution (see the Supporting Information)[29] indicates that the positive charge of the cationic complex is mainly localized on the metal ion (+1.273 e), whereas coordinating O(1), Ow, N(1), and N(2) atoms bear partial negative charges (−0.851, −0.938, −0.605, and −0.633 e, respectively). Wiberg bond indices (WBIs)[30] show that the metal ion is bonded more strongly by the S-donor atoms and the O donor from the 5-Cl-8-HDQ moiety (WBI: Cd–S(1), 0.248; Cd–S(2), 0.247; Cd–O(1), 0.224) relative to the O donor from the coordinated water molecule (WBI: Cd–Ow, 0.140) and the N-donor atoms (Cd–N(1), 0.152; Cd–N(2), 0.109). Interestingly, and in agreement with structural data, an analysis of the WBI matrix shows a weak hydrogen bond between O(1) and H(3A) (O(1)···H(3A) 2.186 Å; O(1)-H(3A)-N(3) 106.7°), reflected in a not negligible WBI of 0.024 between the two atoms. The trend in WBIs is supported by the results of the second-order perturbation analysis of the Fock matrix in the NBO basis, which confirms the strong coordinating ability of S(1) and S(2) atoms. In fact, the interactions between the lone pairs (LPs) localized on the sulfur donor atoms and the unfilled natural orbitals (consisting of the 5s and 5p atomic orbitals (AOs)) of Cd amount to 69.7 and 72.2 kcal mol^{-1}, respectively. The interactions between the three LPs localized on O(1) and the empty AOs on the Cd ion (67.3 kcal mol^{-1}) are furthermore confirmed to be stronger than the Cd–Ow ones (31.3 kcal mol^{-1}), whereas the Cd–N(1) and Cd–N(2) bonds are shown to have a lower energy (33.5 and 24.2 kcal mol^{-1}, respectively).

Single-excitation time-dependent DFT (TDDFT) calculations were also performed to elucidate the electronic structure of the complex and obtain an insight into the nature of the ground and excited states of the complex. The choice of the TDDFT method rather than a wavefunction-based approach, such as CASPT2[31] and SACCI,[32] is because the former can combine an acceptable computational cost with an accurate description of electron correlations and configuration interactions. In fact, this method has been adopted with good results to reproduce the electronic spectra and assign the excited states of many low-spin and closed-shell coordination compounds,[33] including those with Cd^{2+} ions.[34] The pattern of the TDDFT calculated vertical transitions (Table 1) is compared (Figure 2) with the solid-state UV/Vis diffuse reflectance spectrum of $[Cd(\mathbf{L})H_2O](ClO_4)_2$, which is not affected by solvatochromic effects or by the formation of equilibria as the spectra are recorded in solution. There appears to be good agreement between the experimental and calculated data. It should be noted, however, that a quantitative interpretation of UV/Vis spectra is partly prevented by the heavy-atom effect of the Cd^{2+} ion, which could cause singlet transitions of a partial triplet character. TDDFT computations suggest that the band at the lower energy (shoulder at about 480 nm in Figure 2), responsible

Table 1. Main singlet vertical electron transition energies (ΔE) and wavelengths (λ), oscillator strengths (F), configuration interaction coefficients (CI_{coeff}), and assignments calculated at the TDDFT level for $[Cd(\mathbf{L})H_2O)]^{2+}$.[a]

Transition		ΔE [eV] (λ [nm])	F	Excited state (CI_{coeff})[b]	Assignment
A	S0→S1	2.376 (522)	0.026	123→124 (0.664)	5-Cl-8-HDQ (π–π^*)[c]
B	S0→S3	3.740 (332)	0.042	123→127 (0.604)	5-Cl-8-HDQ (π–π^*)[c]
C	S0→S6	4.135 (300)	0.013	123→128 (0.692)	LMCT
D	S0→S8	4.516 (275)	0.077	121→124 (0.546)	5-Cl-8-HDQ (π–π^*)[c]
E	S0→S11	4.698 (264)	0.121	119→124 (0.586)	Py→5-Cl-8-HDQ CT[c]
F	S0→S14	4.919 (252)	0.306	116→124 (0.383)	5-Cl-8-HDQ (π–π^*)[c]
				118→124 (0.411)	Py→5-Cl-8-HDQ CT[c]
G	S0→S20	5.294 (234)	0.096	123→130 (0.588)	5-Cl-8-HDQ (π–π^*)[c]
H	S0→S23	5.431 (228)	0.064	123→131 (0.612)	5-Cl-8-HDQ →3p(S) LP CT[c]

[a] B3LYP functional;[35] Schäfer et al. basis sets for C, H, N, O, S, Cl;[36] LanL2DZ BS with RECP for Cd.[37] Among the various mixing states of each electron transition, only the ones with the highest configuration interaction coefficients are reported for the sake of clarity. [b] See Figure 3 for drawings of the MOs listed below. [c] Py = pyridine fragment within the macrocyclic moiety; 5-Cl-8-HDQ = 5-chloro-8-hydroxyquinoline; CT: charge transfer.

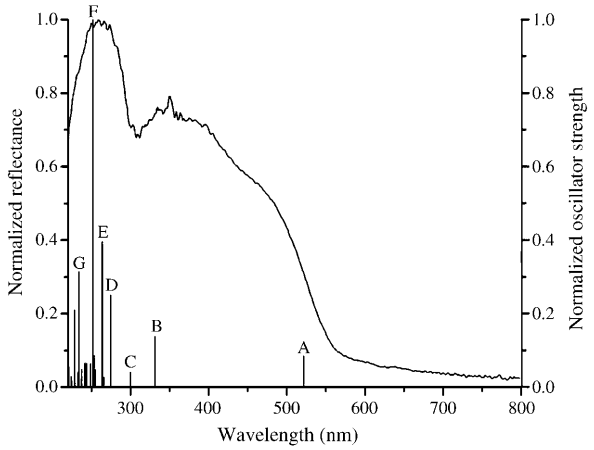

Figure 2. Normalized diffuse reflectance spectrum and TDDFT singlet monoelectronic vertical transitions calculated for $[Cd(\mathbf{L})H_2O)]^{2+}$. Transitions with oscillator strength lower than 2×10^{-3} are not reported for clarity. For transition labeling, see Table 1.

for the orange color of the complex, should be assigned to the S0→S1 transition that results from a π–π^* ^{1}ILCT (intraligand charge transfer) within the 5-Cl-8-HDQ fragment, and corresponds to the pure 123/HOMO→124/LUMO single excitation (transition A in Figure 2, Figure 3, and Table 1). The S0→S3 π–π^* transition B, which involves Kohn–Sham molecular orbitals (MOs) located on the 5-Cl-8-HDQ fragment (mainly corresponding to the 123/HOMO→127/LUMO+3 excitation; Figure 2, Figure 3, Table 1), and the S0→S6 vertical transition C (pure 123/HOMO→128/LUMO+4 excitation), which corresponds to a ^{1}LMCT (ligand-to-metal charge transfer) from the phenyl ring of the 5-Cl-8-HDQ unit to a MO mainly localized on the Cd^{2+} ion, both contribute to the large absorption centered at 360 nm. Finally, several intense vertical transitions (D–H in Figure 2 and Table 1) are calculated to fall in the 4.50–5.80 eV range, thus contributing to the intense absorption at about 260 nm in the experimental reflectance spectrum of the complex. The most intense of these calculated transitions is S0→S14 (transition F in Figures 2 and 3 and Table 1), determined mainly by two one-electron excitations, namely, 116/HOMO-7→124/LUMO (configuration interaction coefficient, $CI_{coeff}=0.383$) and 118/HOMO-5→124/LUMO ($CI_{coeff}=0.411$), the former corresponding to a π–π^* transition localized on the quinolinic rings, the latter involving a CT from the pyridine of the macrocyclic framework to the pyridine ring of the 5-Cl-8-HDQ moiety.

Photophysical properties and NMR investigation of L in aqueous solution, SDS micelles, and liposomes: The absorption and fluorescence bands of **L** are mainly due to the presence in its structure of an 8-HDQ derivative, the photophysical properties of which have been extensively studied.[38,39] The absorption spectrum of **L** in MeCN/H_2O (1:1 v/v) presents a sharp band at 250 nm ($\varepsilon=37000\ dm^3\,mol^{-1}\,cm^{-1}$) and a broad one at 332 nm ($\varepsilon=3100\ dm^3\,mol^{-1}\,cm^{-1}$).[25d] **L** shows a weak emission band centered at 520 nm with a very low

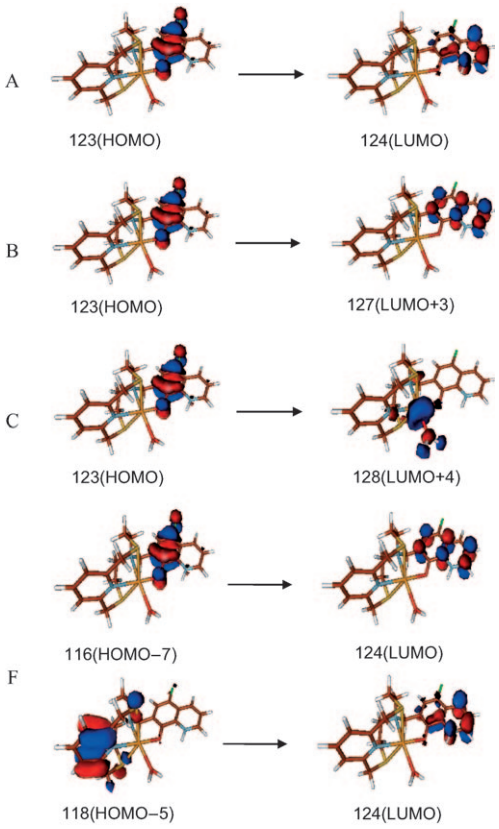

Figure 3. Drawings of the Kohn–Sham MOs calculated for $[Cd(\mathbf{L})H_2O]^{2+}$ involved in the singlet vertical electron transitions A–C and F (see Figure 2 and Table 1) evaluated by TDDFT. Cutoff value = 0.05 e.

fluorescence quantum yield ($\Phi = 0.0001$). According to the literature, low values of fluorescence quantum yields in similar species have been attributed to two different mechanisms, namely, intramolecular photoinduced proton transfer (PPT) between the hydroxyl group and the quinoline nitrogen atom and photoinduced electron transfer (PET) between the nitrogen atom of the macrocycle and the 8-HDQ derivative.[38,39] In addition, in protic media, intermolecular PPT processes involving solvent molecules can also occur, further decreasing the fluorescence quantum yield of this kind of fluorophore.[38,39] Although a significant CHEF effect was observed in the presence of Cd^{2+} in MeCN/H_2O (1:1 v/v) solutions buffered at pH 7.0 with 4-(2-hydroxyethyl)-1-piperazineethanesulfonic acid (HEPES), which corresponded to the formation of the 1:1 Cd^{2+}–**L** complex species (a four times smaller CHEF effect was observed in the presence of Zn^{2+}),[25d] the effects of metal-ion complexation on the absorption properties of **L** in the same medium were in general significant and similar for all the metal ions considered (Cu^{2+}, Zn^{2+}, Cd^{2+}, Hg^{2+}, Pb^{2+}). A significant decrease in the intensity of the bands centered at 250 and 332 nm is accompanied by the appearance of new bands at around 260 and 360 nm,[25d] in agreement with a complexation process involving the deprotonation of the hydroxyl group as already reported[7,38,39] and supported by the structure of $[Cd(\mathbf{L})H_2O]^{2+}$ (see above). The presence of neat isosbestic points indicated that there were no multiple processes but a single conversion process of the free ligand into the complexed one.[25d] These results show that although **L** can bind all the metal ions considered in MeCN/H_2O (1:1 v/v), it selectively turns ON its fluorescence in this medium in the presence of Cd^{2+}. Presumably, under these experimental conditions, both PPT and PET processes are inhibited in the 1:1 complex of **L** with Cd^{2+} (and to a lesser extent in the 1:1 Zn^{2+} complex),[25d] and at the same time Cd^{2+} does not introduce any other possible nonradiative deactivation pathway.

To assess whether **L** could be exploited for probing Cd^{2+} in living cells, we started exploring the spectroscopic and photochemical properties of this ligand in different media in the presence of the initially considered metal ions, Cu^{2+}, Zn^{2+}, Cd^{2+}, Hg^{2+}, and Pb^{2+}, and also including Na^+, K^+, Ag^+, Mg^{2+}, Ca^{2+}, Mn^{2+}, Co^{2+}, Ni^{2+}, Fe^{2+}, Cr^{3+}, and Fe^{3+} as other possible interfering metal ions.

Interestingly, in aqueous solutions buffered at pH 7.4 with 3-*N*-morpholinopropansulfonic acid (MOPS), significant changes in the absorption spectrum of **L** were again observed upon addition of increasing amounts of all the metal ions considered (see Figure 4 for the case of Cd^{2+}), with the exception of Na^+, K^+, Ca^{2+}, and Mg^{2+}, for which changes were very small, whereas the ligand maintained its OFF state of fluorescence in the presence of all the metal ions considered, including Cd^{2+}. It appears, therefore, that **L** gives a Cd^{2+}-selective response in terms of enhancement of fluorescence emission in more lipophilic environments in which the PPT processes are inhibited. We then decided to investigate the optical response of **L** by adding increasing

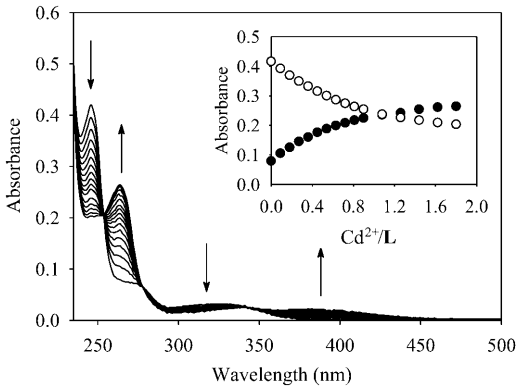

Figure 4. Changes in the absorption spectrum of **L** (1.22×10^{-5} M, H_2O, pH 7.4, MOPS, 25 °C) upon addition of increasing amounts of a solution of Cd^{2+} (1.10×10^{-3} M in H_2O; see the Supporting Information), with isosbestic points at 253, 278, and 343 nm. Inset: absorbance at 264 (●) and 245 nm (○) ($\log K_{ass} = 6.2(1)$ evaluated using Hyperquad).[40] K_{ass} = association equilibrium constant.

amounts of Na^+, K^+, Ag^+, Mg^{2+}, Ca^{2+}, Mn^{2+}, Co^{2+}, Ni^{2+}, Fe^{2+}, Cu^{2+}, Zn^{2+}, Cd^{2+}, Hg^{2+}, Pb^{2+}, Cr^{3+}, or Fe^{3+} in the presence of SDS micelles or liposomes, at physiological pH, as systems mimicking cell membranes and, in general, the intracellular environment.[41] Spectrophotometric and spectrofluorimetric titrations of **L** with the aforementioned metal ions were performed in aqueous solutions (25 °C) buffered at pH 7.4 with MOPS, and containing SDS at a concentration corresponding to the critical micelle concentration (see Experimental Section).[42,43] Significantly, also under these conditions, we observed changes in the absorption spectrum of **L** on adding increasing amounts of all the considered metal ions, which were very similar to those recorded in buffered aqueous solutions (Figure 4, Figure 5A). In the cases of Na^+, K^+, Ca^{2+}, and Mg^{2+}, no changes at all were observed in the absorption spectrum of **L** (see the Supporting Information).

Nevertheless, in the presence of SDS micelles only the complexation of Cd^{2+} is accompanied by a CHEF effect (Figure 5B and the Supporting Information), and as expected the best fitting of the fluorescence relative intensity versus molar ratio plot (Figure 5C) indicates the formation of a complex cation with a 1:1 metal-to-ligand stoichiometry during the spectrofluorimetric titration. In the presence of SDS micelles, Zn^{2+} did not have any effect on the fluorescence emission of **L**, contrary to what was observed in MeCN/H_2O (1:1 v/v)[25d] and in agreement with the fact that the medium, in particular nanosized containers such as micelles and liposomes (see below), can have a profound influence on the photophysical properties of an emitting species.[41] Interestingly, free **L** in SDS micelles is slightly luminescent (see Figure 5B), as observed in organic polar aprotic solvents, which inhibit intra- and intermolecular PPT processes. This would indicate that **L** and its Cd^{2+} complex prefer to stay within the SDS micelles in a more lipophilic environment. Furthermore, the emission band of **L** in SDS micelles blueshifts upon complexation with Cd^{2+}. This could

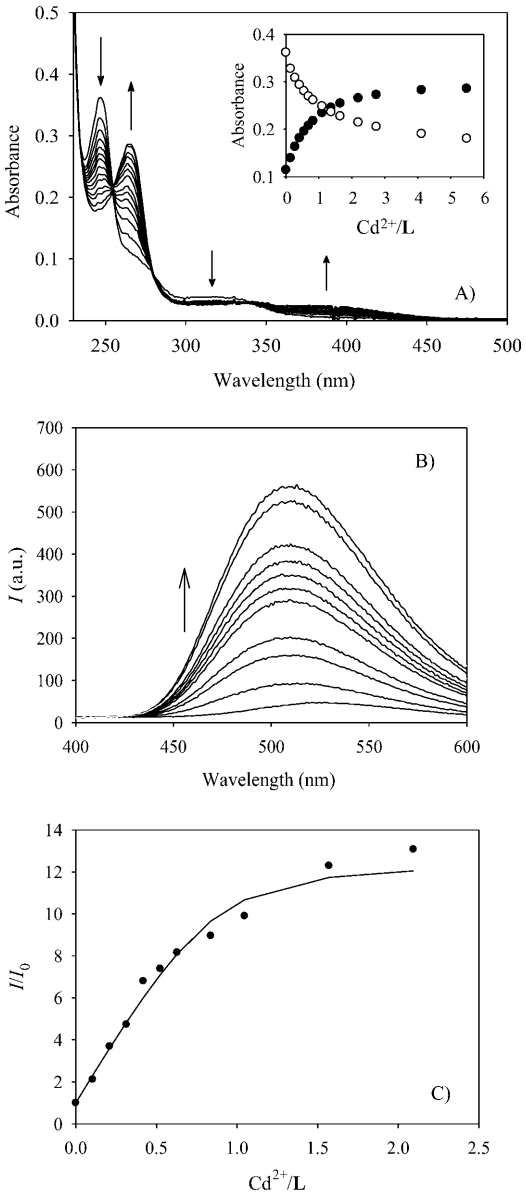

Figure 5. A) Changes in the absorption spectrum of **L** (1.22×10^{-5} M, H_2O, pH 7.4, MOPS, 25 °C), in the presence of SDS micelles (see the Experimental Section), upon addition of increasing amounts of a solution of Cd^{2+} (1.10×10^{-3} M in H_2O; see the Supporting Information), with isosbestic points at 253, 278, and 338 nm. Inset: absorbance at 264 (●) and 245 nm (○) ($\log K_{ass}=5.4(1)$ evaluated using Hyperquad).[40] B) Fluorescence emission spectra of **L** (1.22×10^{-5} M, H_2O, pH 7.4, MOPS, 25 °C, $\lambda_{exc}=332$ nm) in H_2O solution in the presence of SDS micelles on adding increasing amounts of a solution of Cd^{2+} (1.10×10^{-3} M in H_2O; see the Supporting Information). C) Fluorescence relative intensity I/I_0 (at 510 nm) versus molar ratio for the titration shown in (B) ($\log K_{ass}=6.0(1)$ evaluated using SPECFIT).[44]

be explained by considering that the excited states of the Cd^{2+} complex with **L** are characterized by a strong charge separation, and are therefore destabilized by the low polar and aprotic micelle environment.

In this context, it seemed interesting to ascertain the actual location of **L** and its Cd^{2+} complex when dispersed in a SDS micellar solution by measuring their self-diffusion coefficients through pulsed field-gradient stimulated echo (PFGSTE) NMR experiments.[45] Due to the high lipophilicity of **L** and in consideration of the well-known relatively high concentrations required for NMR measurements, both the ligand and the complex were dissolved in a D_2O/DMSO solvent mixture (6:1, 0.7 mL) buffered with Dulbecco's phosphate-buffered saline (DPBS) and containing SDS (0.16 M). Two PFGSTE experiments were carried out, one on an **L**/SDS mixture and the other on an **L**/Cd^{2+}/SDS mixture.

The ^{1}H NMR spectrum (aromatic region) of **L** (2.5×10^{-3} M) in the presence of Cd^{2+} (2.5×10^{-3} M) and SDS is shown in Figure 6B, whereas Figure 6A shows the ^{1}H NMR spectrum of **L** (aromatic region) in the presence of only SDS, both integrating for eight protons. The doublet at 7.49 ppm for the **L**/SDS system (ascribed to the equivalent protons of the pyridinic ring of **L**), the multiplet at 7.67 ppm for the **L**/Cd^{2+}/SDS system, and the triplet at 0.94 ppm belonging to the SDS terminal methyl group in both mixtures were used to follow the signal decay upon increasing the gradient strength. Experimental results are shown in Figure 7. According to Equation (1) (see Experimental Section), data were fitted through a monoexponential function ($R=0.999$ in all cases) and the self-diffusion coefficients calculated for the SDS in both mixtures (D_{SDS}), for **L** in the presence of SDS ($D_{\mathbf{L}}$), and for **L** in the presence of Cd^{2+} and SDS ($D_{Cd^{2+}/\mathbf{L}}$) were almost identical and ranged between 4.8×10^{-11} and 5.2×10^{-11} m^2s^{-1}. Such self-diffusion coefficients are representative of a molecular aggregate, and indicate that independently of the presence of the DMSO in solution, the SDS molecules still organize themselves into micelles.

From data reported in the literature,[46] the viscosity (η) of the solvent mixture used was determined as 1.707 mPa. It is

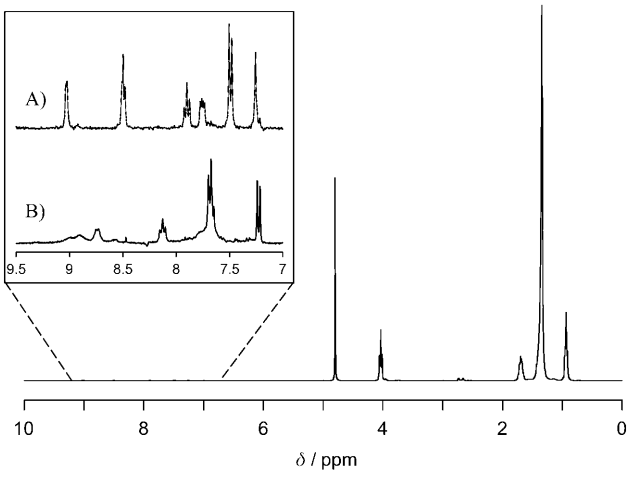

Figure 6. ^{1}H NMR spectrum of **L** (2.5×10^{-3} M) in a D_2O/DMSO (6:1) solvent mixture buffered with DPBS at 25 °C, A) in the presence of SDS (0.16 M) and B) in the presence of Cd^{2+} (2.5×10^{-3} M) and SDS (0.16 M). Signals are referred to the residual protons of the deuterated water (4.8 ppm).

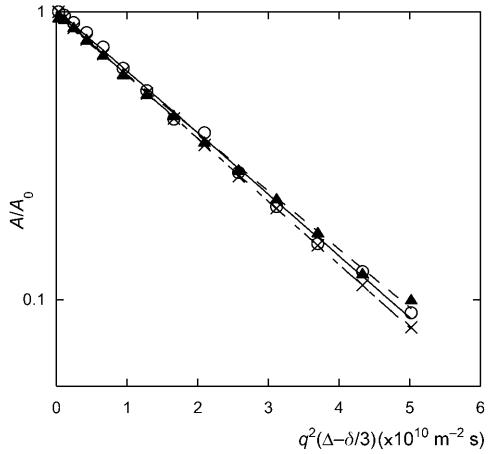

Figure 7. Semilog plot of SDS (0.94 ppm in the mixture **L**/SDS, (○)) and **L** (7.49 ppm in the mixture **L**/SDS, (×); 7.67 ppm in the mixture **L**/Cd^{2+}/SDS, (▲)) ^{1}H NMR signal decay versus $q^2(\Delta-\delta/3)$ as detected in the PFGSTE experiments (see Experimental Section and Discussion).

worth recalling that the translational displacement of an object (i.e., a molecule/molecular aggregate) in solution is inversely related to its hydrodynamic radius (R_h) through the Stokes–Einstein equation ($D=k_BT/6\pi\eta R_h$, in which k_B is the Boltzmann constant and other symbols have their usual meaning). Hence, from D_{SDS} an R_h of 2.6 nm can be calculated, in excellent agreement with the radius of an SDS-based spherical micelle.

On the contrary, the expected self-diffusion coefficient for a simple molecular dispersion of **L** or a 1:1 complex between Cd^{2+} and **L** in aqueous solution may be easily estimated at around one order of magnitude higher than observed here. This remark, along with the identical values found for D_{SDS}, $D_{\mathbf{L}}$, and $D_{Cd^{2+}/\mathbf{L}}$, definitely proves the confinement of **L** and its 1:1 complex with Cd^{2+} within the SDS micellar aggregates. Moreover, both the results from the previously discussed fluorescence analysis and the very low solubility of **L** in aqueous environments strongly suggest that such a molecule is buried in the hydrophobic micellar core.

Based on these results, we performed spectrofluorimetric titrations in aqueous solutions (25 °C) buffered at pH 7.4 with MOPS and containing liposomes. The results obtained were very similar to those recorded in the presence of SDS micelles. As regards the absorbance data, we could only obtain qualitative information from them. In fact, solutions containing liposomes were milky opalescent and consequently exhibited high values of scattered light. The absorption bands of **L** and of its complexes were therefore partially covered by a ground noise and we could only distinguish the very tops of the UV bands, which, however, changed in line with what was observed in the presence of the SDS micelles. As a matter of fact, the maximum at about 250 nm decreased, whereas the new band centered at about 260 nm increased on adding increasing amounts of all metal ions considered (again with the exception of Na^+, K^+, Ca^{2+}, and Mg^{2+}). As far as emission changes are concerned, a significant CHEF effect was observed only upon addition of Cd^{2+} (Figure 8). The inflection point in the fluorescence relative intensity versus molar ratio plot (Figure 8B) confirms the formation of a 1:1 metal-to-ligand complex cation during the spectrofluorimetric titrations. The fluorescence state of **L** in the presence of liposomes is not altered in the presence of the other considered metal ions. The fluorescence intensity of free **L** in the presence of liposomes and its slight blue-shift observed on adding Cd^{2+} (Figure 8A) indicate that **L** and its 1:1 Cd^{2+} complex (Figure 8B) are located within the phospholipid bilayer vesicles, in an environment similar to that experienced in the SDS micelles. As regards the affinities of **L** for Cd^{2+} under the different tested conditions, from the normalized fluorescence intensity versus molar ratio plots obtained by spectrofluorimetric titrations (see Figures 5C and 8B) we calculated values for $\log K_{ass}$ of 6.0(1) and 5.9(1) in the presence of SDS micelles or liposomes, respectively (K_{ass} = association equilibrium constant). Interestingly, these values were very close to that calculated from a spectrophotometric titration in H_2O in the absence of both SDS and liposomes ($\log K_{ass}=6.2(1)$, Figure 4), but lower than the value of the formation constant for the 1:1 complex between Cd^{2+} and **L** calculated potentiometrically in MeCN/H_2O (1:1 v/v) [$\log K=9.33(5)$].[25d]

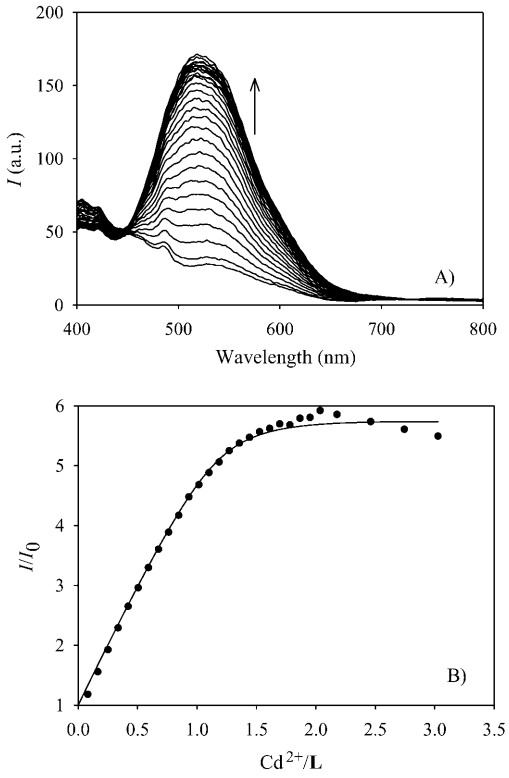

Figure 8. A) Fluorescence emission spectra of **L** (4.64×10^{-5} M, H_2O, pH 7.4, MOPS, 25 °C, $\lambda_{exc}=332$ nm) in a suspension of liposomes in H_2O (30 μL, 10 mg mL^{-1}, of a liposome suspension in DPBS were added to 2.5 mL of the solution of **L**) on adding increasing amounts of a solution of Cd^{2+} (3.29×10^{-3} M) in H_2O (see the Supporting Information). B) Fluorescence relative intensity (at 520 nm) versus molar ratio for the titration shown in (A) ($\log K_{ass}=5.9(1)$ evaluated using SPECFIT).[44]

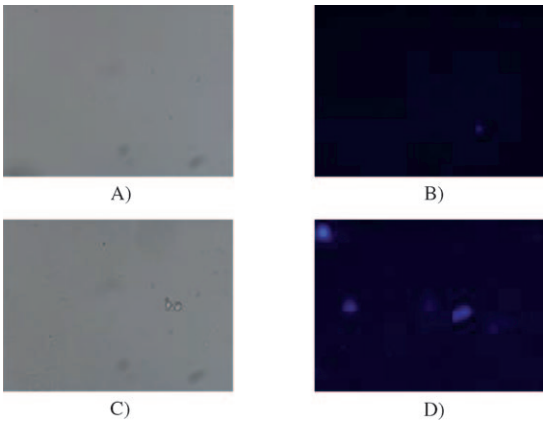

Figure 9. Visualization of a suspension of liposomes (50 μL, 10 mg mL^{-1} in DPBS) in the presence of **L** (A,B) and of **L** and Cd^{2+} (C,D) in A,C) phase-contrast mode and B,D) fluorescence mode (see Experimental Section for technical details concerning image collection).

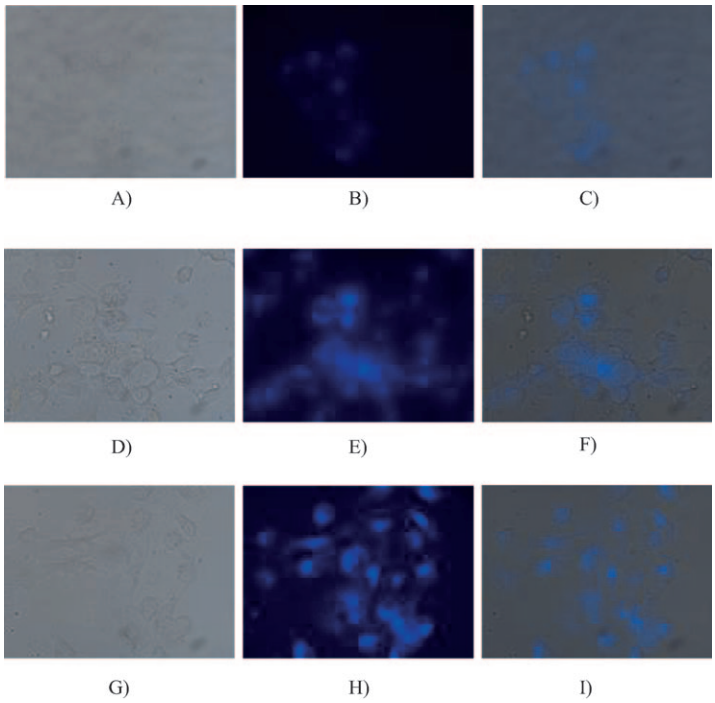

Figure 10. Visualization of a Cos-7 cell control culture (A,B,C), of a Cos-7 cell culture in the presence of **L** (D,E,F), and of a Cos-7 cell culture preincubated with Cd^{2+} and in the presence of **L** (G,H,I). Images were obtained in phase-contrast mode (A,D,G), in fluorescence mode (B,E,H), and in a merge mode (C,F,I) (see Experimental Section for technical details concerning image collection).

The ability of **L** to respond to the presence of Cd^{2+} in liposomes can easily be assessed by fluorescence microscopy. Figure 9 shows fluorescence microscopy images of two samples of a liposome suspension in DPBS in the presence of **L**, one of which was enriched with Cd^{2+}. In both cases, no self-fluorescence is observed and the fluorescence emission, which is very intense in the presence of Cd^{2+}, is confined within the phospholipid bilayer vesicles. The images in Figure 9 also show that no fluorescence emission is present in the environment surrounding the liposomes, and this visually demonstrates that **L** and its Cd^{2+} complex prefer more lipophilic environments.

Intracellular fluorescence measurements: Encouraged by the very promising results so far discussed, we next sought to evaluate the ability of **L** as a fluorescent probe to sense Cd^{2+} within cells by fluorescence microscopy and flow cytometry. Possible interference by Zn^{2+}, only observed in MeCN/H_2O (1:1 v/v) and not in the presence of micelles and liposomes, has to be ruled out in vitro as the level of free Zn^{2+} within cells is extremely low ($\approx 10^{-8}$ M) and,[47] furthermore, the response of **L** to the presence of Cd^{2+} is in any case significantly higher.

HL-60, Cos-7, and Saos-2 cells were chosen because they represent good models and are already widely used in Cd^{2+} toxicity experiments.[48] Fluorescence microscopy images of Cos-7 cells (see Experimental Section) in a control experiment without incubation with **L** and Cd^{2+} show no background fluorescence, but some self-fluorescence is observed within the cellular environment (Figure 10 A–C). Cos-7 cells incubated with **L** for 5 min at 25 °C (see Experimental Section) show higher homogeneously distributed intracellular fluorescence, and still no background fluorescence (Figure 10 D–F). Therefore, **L** is cell-permeable and appears to diffuse within the cell environment without a district preference. The observed luminescence, therefore, can be explained by the partially lipophilic environment that **L** finds inside the cells. We have already discussed the typical luminescence (though very weak) of the free ligand under moderately polar conditions (see the previous section, examples with SDS and liposomes). Supplementing cells with 50 μM $CdCl_2$ in the growth medium for 2 h at 37 °C and then staining them with **L** (see Experimental Section for details of conditions) resulted in a marked increase in observed intracellular fluorescence (Figure 10 H and I). Furthermore, in the presence of Cd^{2+} within the cells, the fluorescence emission appears to be more localized in specific intracellular areas, as if Cd^{2+} prefers to accumulate in determined intracellular districts. Taken together, these fluorescence microscopy experiments on fixed Cos-7 cells show that **L** is cell-permeable and can respond specifically to changes in intracellular Cd^{2+} levels.

By further using confocal microscopy measurements, we probed the ability of **L** to track Cd^{2+} in living cells, not only in fixed ones, which, as is well known, are usually much more permeable. Saos-2 cells incubated with 10 μM **L** for up to 10 min at 25 °C show negligible intracellular fluorescence in the perinuclear region (Figure 11 A). On the contrary, cells treated first with 50 μM $CdCl_2$ and then with 10 μM **L** (see Experimental Section) show enhanced cytosolic fluorescence (Figure 11 B). Again in these cells fluorescence appeared to be localized in bright spots rather than diffused in the cytoplasm.

Cytofluorimetric analyses of leukemic HL-60 cells loaded with **L** and counterstained with propidium iodide (PI) al-

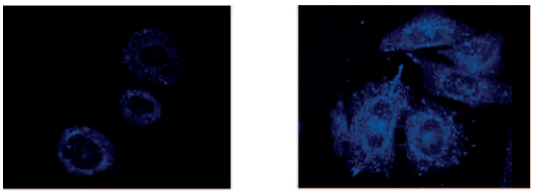

Figure 11. Confocal fluorescence images of Cd^{2+} in Saos-2 cells: A) cells incubated with 10 μM **L** for 10 min in the dark at 25 °C; B) cells incubated for 30 min at 37 °C with 50 μM $CdCl_2$, washed with DPBS, and then incubated with 10 μM **L** for 10 min in the dark at 25 °C (see Experimental Section for technical details concerning image collection). The images were collected by a Nikon C1s confocal laser-scanning inverted microscope, with the excitation light at 405 nm and the emission light at 515–530 nm.

lowed discrimination of viable from damaged cells and the selective analysis of intracellular **L** fluorescence. Five cell cultures were prepared containing, respectively, 0, 10, 50, 100, and 1000 μM $CdCl_2$. Figure 12 shows the control cytograms (top), and the cytograms of cells treated overnight with Cd^{2+} up to a concentration of 100 μM (middle) and up to 1000 μM (bottom). It can be seen that **L** is not only retained in living cells (quadrant d), but also in damaged cells (quadrant b), whereas dead cells do not seem to accumulate any **L** because no fluorescence was detected. Figure 12 also shows clearly that **L** had no toxic effects on the cells. Interestingly, Cd^{2+} induced a detrimental effect only in the cells treated overnight with the higher dose: dead and damaged cells were in fact between about 15 and 20 % in the samples treated with Cd^{2+} up to a concentration of 100 μM, whereas they reached 80 % in the samples treated with Cd^{2+} up to 1000 μM.

On analyzing the fluorescence distribution of **L** in viable cells (see Table 2 and the Supporting Information), we found that there was a proportional increase in the fluorescence intensity distribution of **L** on increasing the concentration of Cd^{2+} used for cell culturing.

Table 2. Fluorescence intensity of **L** (logarithmic scale), calculated as a geometric mean of the cellular **L** fluorescence distribution in a cytometric assay, in viable leukemic HL-60 cells incubated with increasing amounts of Cd^{2+}.[a]

Control cells	Cd^{2+} 10 μM	Cd^{2+} 50 μM	Cd^{2+} 100 μM	Cd^{2+} 1000 μM
18.39	18.71	20.73	22.86	30.75

[a] See the Experimental Section and Supporting Information.

Conclusion

We have shown the photochemical characterization and application of the chemosensor **L** in living-cell imaging in vitro. In particular, although this probe, which is readily permeable to cells, can complex all the metal ions considered, it shows a chelation-induced enhancement of its fluorescence in buffered solutions containing SDS micelles or liposomes only upon formation of a 1:1 complex with Cd^{2+} ions. The

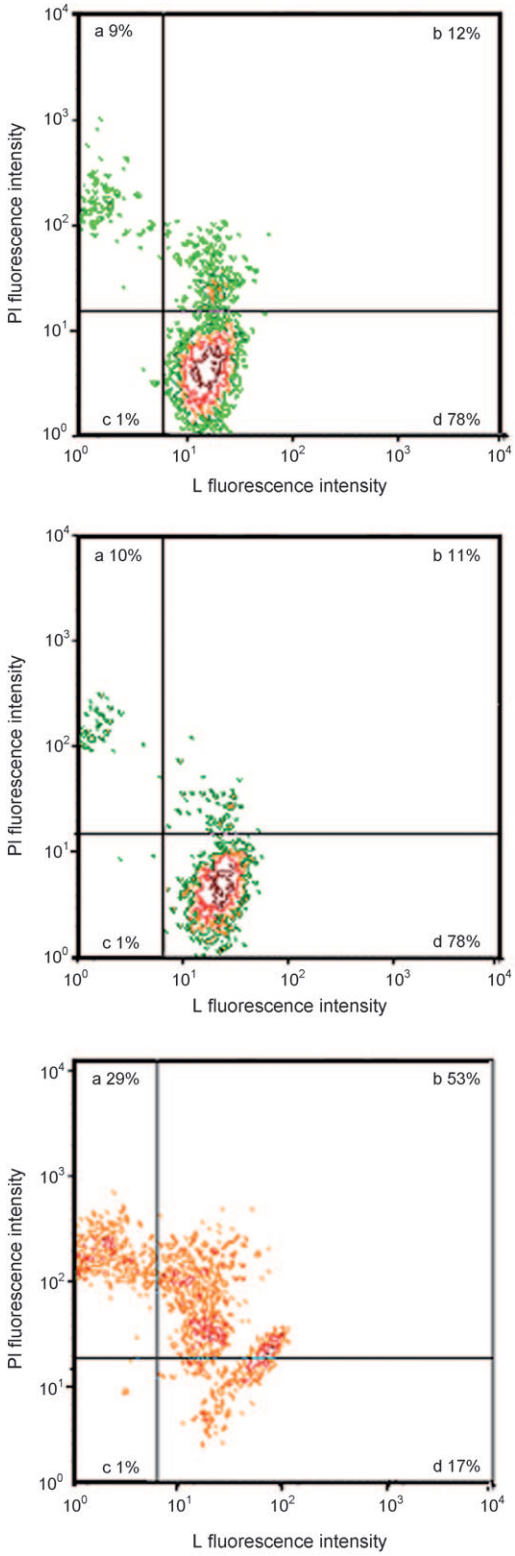

Figure 12. Flow cytometric evaluation of **L** fluorescence and cell viability in control HL-60 cells (top), and in cells treated with 100 μM $CdCl_2$ (middle) and 1000 μM $CdCl_2$ (bottom) (see Experimental Section for technical details concerning measurements). Quadrant a: dead cells (positive to PI, negative to **L**); quadrant b: damaged cells (positive to PI and **L**); quadrant d: viable cells (negative to PI, positive to **L**); quadrant c: cellular debris. The percentage of cells localized in each quadrant is indicated.

observed affinity toward cadmium(II) ions under these conditions ($K_{ass} \approx 10^6\,M^{-1}$) and the increase in fluorescence intensity are sufficiently high to allow the imaging of Cd^{2+} in viable cells in vitro. This conclusion is supported by intracellular fluorescence measurements in different cellular families. These measurements show that **L** does not present cytotoxic effects, that it has very low background fluorescence in the absence of Cd^{2+}, but it becomes very bright only in cells loaded with this ion. Interestingly, **L** is also able to detect intracellular Cd^{2+} in fixed cells, thus making its application field wider and less dependent on the complex apparatus for viable cell microscopy.

Furthermore, **L** can be used for qualitative/quantitative determinations of Cd^{2+} by flow cytometry or fluorescence microscopy because **L** selectively stains living cells and its fluorescence signal is directly correlated with Cd^{2+} content in cells. We also wish to point out the extreme versatility and usefulness of 8-HDQ and its derivatives in the field of supramolecular chemistry and molecular sensors. 8-HDQ is experiencing a renaissance in synthetic coordination chemistry: it has long been known to the chemist community only as an excellent analytical reagent and versatile ligand for many metal ions, and has only recently been considered a valuable starting fluorescent platform around which to develop extremely selective fluorescent chemosensors for in vivo mapping of different metal ions.

Experimental Section

General methods and materials: All melting points are uncorrected. Microanalytical data were obtained by using a Fison EA CHNS-O instrument ($T = 1000\,°C$). Infrared spectra were recorded on a Bruker IFS55 spectrometer at room temperature, after purging the sample cell with a flow of dried air.

All reagents were purchased from Sigma and were Ultrapure grade. **L** was synthesized according to literature procedures.[25d] Solvents used were DMSO (Merck UVASOL) and Millipore-grade water. DPBS without Ca^{2+} and Mg^{2+} (8 g L^{-1} NaCl, 0.20 g L^{-1} KCl, 0.20 g L^{-1} Na_2HPO_4, and 0.20 g L^{-1} KH_2PO_4, pH 7.2) was prepared in doubly distilled water.

Liposomes were prepared by the thin-layer evaporation technique.[49] Phosphatidylcholine from egg yolk (Aldrich) was dissolved in $CHCl_3$ (10 mg mL^{-1}) and the solvent removed under reduced pressure to obtain a thin film on the sides of the flask. The film was left under vacuum overnight to remove all traces of the organic solvent. The resulting dried lipid film was dispersed with DPBS (1 mL). The mixture was vortexed and sonicated to give small unilamellar vesicles (SUVs).

Synthesis of $[Cd(L)H_2O](ClO_4)_2 \cdot MeCN$: Solid $Cd(ClO_4)_2 \cdot 6H_2O$ (19.3 mg, 0.046 mmol) [**Caution!** The unpredictable behavior of perchlorate salts requires extreme care in handling.] was added to a suspension of **L** (20 mg, 0.046 mmol) in MeCN (3 mL). On stirring the reaction mixture for 2 h at room temperature, the ligand went into solution and the mixture turned orange. Crystals of the complex were obtained by diffusion of Et_2O into the reaction mixture (15 mg, 41% yield). M.p. 210 °C with decomposition; ^1H NMR (300 MHz, $[D_3]$MeCN, 25 °C, TMS): $\delta = 2.10$–2.30 (m, 2H), 2.5–2.7 (m, 4H), 3.00–3.20 (m, 2H), 3.82 (s, 2H), 4.24 (d, J (H,H) = 17.1 Hz, 2H,), 4.41 (d, J(H,H) = 16.8 Hz, 2H), 7.55 (d, J (H,H) = 7.8 Hz, 2H), 7.65 (s, 1H), 7.90–8.10 (m, 2H), 8.97 (d, J (H,H) = 4.5 Hz, 1H), 9.16 ppm (d, J(H,H) = 7.8 Hz, 1H); FTIR (KBr): $\tilde{\nu} = 3096$, 2850, 1618, 1597, 1574, 1534, 1453, 1395, 1314, 1088, 923, 798, 736, 624 cm^{-1}; UV/Vis (MeCN): λ_{max} (ε) = 250 (28800), 264 (20150), 332 (2500), 380 (1300), 460 nm (400 $mol^{-1}\,dm^3\,cm^{-1}$); elemental analysis calcd (%) for $C_{23}H_{27}CdCl_3N_4O_{10}S_2$: C 34.40, H 3.35, N 6.95, S 8.00; found: C 34.43, H 3.39, N 6.98, S 7.99.

X-ray crystallography: The single-crystal data for $[Cd(L)H_2O](ClO_4)_2 \cdot MeCN$ were collected by ω scans and graphite-monochromated $Mo_{K\alpha}$ radiation ($\lambda = 0.71073$ Å) on an APEX II CCD diffractometer at 294(2) K. The dataset was corrected for Lorentz polarization effects and for absorption by using *SADABS*.[50] The structure was solved by direct methods with *SIR-97*[51] and refined by using *SHELXL-97*.[52] All non-hydrogen atoms were refined anisotropically. All the hydrogen atoms were located from difference maps; however, they were introduced at calculated positions and refined by a riding model, except those on the coordinated water molecule, which were refined isotropically by restraining the O–H distances. The MeCN molecule displays two different orientations of almost equal probability (occupancy 0.5): this model of disorder was refined with no restraints, and no H atoms were located on the MeCN molecule. $[Cd(L^6)H_2O](ClO_4)_2 \cdot MeCN$: $C_{23}H_{27}CdCl_3N_4O_{10}S_2$; $M_w = 802.36$; monoclinic; space group $C2/c$ (No. 15); $a = 25.459(5)$, $b = 13.655(3)$, $c = 17.322(4)$ Å; $\beta = 90.94(3)°$; $V = 6021(2)$ Å^3; $Z = 8$; $\rho_{calcd} = 1.770$ g cm^{-3}; $2\theta_{max}$ 58.42°; $\mu(Mo_{K\alpha}) = 1.191$ mm^{-1}; orange platelet crystals ($0.12 \times 0.08 \times 0.02$ mm^3). Empirical absorption corrections (T_{min} 0.864, T_{max} 0.976); 24430 measured reflections; 7838 unique reflections ($R_{int} = 0.0716$) of which 3992 had [$I > 2\sigma(I)$]. The weighting scheme $w^{-1} = [\sigma^2(Fo)^2 + (0.0719k)^2]$ in which $k = 1/3(Fo^2 + 2Fc^2)$ was applied. At final convergence R_1 [$I > 2\sigma(I)$] = 0.0526; wR_2 (all data) = 0.1456 for 419 refined parameters; $S = 0.911$; $(\Delta/\sigma)_{max} = 0.013$; $\Delta\rho_{max} = 0.93$ e Å^{-3}. CCDC-728181 contains the supplementary crystallographic data for this paper. These data can be obtained free of charge from The Cambridge Crystallographic Data Centre via www.ccdc.cam.ac.uk/data_request/cif.

Photophysical measurements: Absorption spectra were recorded at 25 °C by using a Varian model Cary 5 UV/Vis–NIR spectrophotometer and a Thermo Nicolet Evolution 300 spectrophotometer. Uncorrected emission spectra were obtained with a Varian Cary Eclipse spectrofluorimeter. To allow comparison among emission intensities we performed corrections for instrumental response, inner filter effect, and phototube sensitivity.[53] A correction for differences in the refractive index was introduced when necessary. Spectrophotometric and spectrofluorimetric titrations of **L** with metal ions at 25 °C were performed by the addition of increasing volumes of an aqueous solution of the metal ion to a solution of the ligand (3 mL) buffered at pH 7.4 with MOPS (1 M, 3 μL, H_2O).

Ligand solution concentrations were maintained during titrations in the range 4.64×10^{-5}– 1.22×10^{-5} M and were prepared by dissolving **L** in few drops of DMSO in precalibrated 50.0 or 100.0 mL volumetric flasks and adding water to the mark. The concentration of metal-ion solutions in H_2O used for the titrations ranged between 6.0×10^{-4} and 1.10×10^{-3} M. For titrations in the presence of SDS, a solution of SDS (50 μL, 0.5 M) in DPBS was added to the solution of **L** (3 mL, see above) to reach a final concentration for the SDS that was slightly higher than the critical micelle concentration (8.0×10^{-3} M).[42,43] For titrations in the presence of liposomes, a suspension of liposomes in DPBS (30 μL, 10 mg mL^{-1}) was added to the solution of **L** (2.5 mL, see above). Titration data are reported in the Supporting Information.

NMR measurements: ^1H NMR measurements were performed on a Bruker Avance 300 MHz (7.05 T) spectrometer equipped with a field-gradient probe (DIFF30) supplied by a Bruker Great 1/40 amplifier that could generate field gradients up to 1200 G cm^{-1}. Self-diffusion experiments were carried out at (25 ± 0.1) °C by means of the PFGSTE sequence[45] with two gradient pulses of duration δ, separation Δ, and strength g. The ^1H NMR signal decay A in such NMR experiments is given by Equation (1):

$$\ln\left(\frac{A}{A_0}\right) = -D(\gamma g \delta)^2\left(\Delta - \frac{\delta}{3}\right) = -Dq^2 t_D \qquad (1)$$

in which A and A_0 are the NMR signal intensities in the presence and absence, respectively, of the applied field gradient, γ is the ^1H gyromagnetic ratio, $t_D = (\Delta - \delta/3)$ is the diffusion time, and the coefficient $q = \gamma g \delta$ represents the so-called "scattering vector". The signal attenuations were measured by recording the signal intensity in the ^1H NMR spectra. Experi-

ments were carried out by varying the magnitude of the applied magnetic field gradient g, while keeping δ and Δ constant during each experimental run. Equation (1) predicts that the self-diffusion coefficient D can be extracted from the slopes of the attenuation profiles obtained from the exponential regression of A/A_0 as a function of q^2t_D at fixed δ and t_D. Reproducibility, as estimated from repeated measurements, was evaluated within 4%. The solutions (0.7 mL) for PFGSTE experiments were prepared by mixing D_2O (0.4 mL), DMSO (0.1 mL), and SDS solution (0.2 mL, 0.5 M) in DPBS (prepared in D_2O). In this mixture, [**L**] and $[Cd^{2+}]$ were 2.5×10^{-3} M.

Cell culture: HL-60 (human promyelocytic leukemia), Saos-2 (human osteogenic sarcoma), and Cos-7 (African Green Monkey SV40-transfected kidney fibroblast cell line) cells were routinely cultured in RPMI 1640 medium (Gibco, UK) supplemented with 10% heat-inactivated fetal calf serum (FCS) (Euroclone, UK) and L-glutamine (2 mM; Gibco, UK) at 37 °C in 5% CO_2 atmosphere.

Fluorescence measurements and imaging of cells: For flow cytometric assays, HL-60 cells were seeded at 10^5 cells mL^{-1} and allowed to grow for 48 h. Five cell cultures of this kind were prepared containing $CdCl_2$ at 0, 10, 50, 100, and 1000 μM, respectively. These cell cultures were incubated overnight at 37 °C in 5% CO_2 atmosphere, and then a solution of **L** was added to reach a final concentration of 10 μM in each culture. Cells were counterstained by 7 μM PI to discriminate dead cells.

Flow cytometric measurements were performed on a Bryte HS cytometer (BioRad, UK) equipped with a Hg lamp and a filter set with an excitation band centered at 360 nm and two emission bands centered, respectively, at 500 nm (**L** fluorescence) and 600 nm (PI fluorescence). Fluorescence signals were acquired on logarithmic scale, and analyzed by means of WinMDI software. A contour plot was used to determine the percentages of viable cells (negative to PI, positive to **L**), dead cells (positive to PI, negative to **L**), damaged cells (positive to PI and **L**), and cellular debris (negative to PI and **L**). A gating was imposed on viable cells, identified as those excluding PI. The mean fluorescence intensity of these viable cells was calculated as a geometric mean of the cellular **L** fluorescence distribution.

For fluorescence microscopy on cells, Cos-7 cells were seeded on WillCox plates (WillCo Wells BV, The Netherlands) at 3×10^4–5×10^4 cells cm^{-2}. $CdCl_2$ (50 μM) was added to the cells, which were incubated for 2 h at 37 °C in a 5% CO_2 atmosphere. The cells were washed three times with DPBS and fixed with MeOH/acetone (1:1; previously cooled at −20 °C) for 2 min.[54] The plates were then left to dry in an air atmosphere. **L** (10 μM) was then added and the plates were left for 5 min in the dark at 25 °C. Control experiments were performed by adding only **L** without preincubation with Cd^{2+}.

For fluorescence microscopy on liposomes, two samples of a liposome suspension were analyzed. Concentrated **L** (10 μL) was added to both samples of liposomes (50 μL, 10 mg mL^{-1} of a suspension in DPBS), one of which was also enriched with $CdCl_2$ (1.0×10^{-2} M, 1 μL). The fluorescence images of Cos-7 and liposomes were observed under a Nikon Eclipse 90i microscope equipped with a Nikon Digital Sight DS-5M telecamera, an excitation band-pass filter centered at 365 nm, and an emission long-pass filter at over 397 nm.

For confocal fluorescence microscopy, Saos-2 cells were seeded on WillCox plates (WillCo Wells BV, The Netherlands) at 10^4 cells cm^{-2} and allowed to grow for 48 h before experiments were performed. Cells were then incubated with 50 μM $CdCl_2$ for 30 min at 37 °C in a 5% CO_2 atmosphere. The cells were washed three times with DPBS, treated with 10 μM **L**, incubated for 10 min in the dark at 25 °C, and then placed on the microscope stage for imaging. Control experiments were performed by adding only **L** without preincubation with Cd^{2+}. The images were collected at 515–530 nm emission and at 405 nm excitation using a Nikon C1s confocal laser-scanning inverted microscope, equipped with a Nikon PlanApo 60, 1.4 NA (numerical aperture) oil-immersion lens.

DFT calculations: Quantum-chemical calculations were performed at the DFT level[27] on the two N- and O-protonated isomers of the complex cation $[Cd(\mathbf{L})H_2O]^{2+}$ with the commercial suite of programs Gaussian 03,[55] by using the B3LYP hybrid functional.[35] Although all-electron basis sets (BSs) provide better accuracy, pseudopotential techniques are useful when relativistic effects must be taken into account. Thus, the double-ζ plus polarization all-electron (pVDZ) BSs by Schäfer et al.[36] were used for C, H, N, S, and O, whereas the LanL2DZdp BS with relativistic effective core potentials (RECP)[37] was used for Cd.[56,57] After a geometry optimization (see the Supporting Information) starting from structural data, NBO charge distributions (see the Supporting Information)[29] and WBIs[30] were calculated. Electronic transition energies and oscillator strengths were calculated at the TDDFT level (35 states). The program Molden 4.7 was used to investigate charge distributions and Kohn–Sham MO shapes.[58]

Acknowledgements

MIUR is gratefully acknowledged for financial support (Project PRIN 2007C8RW53). We gratefully acknowledge Dr. Chiara Mangano from the Department of Biochemistry "G. Moruzzi", University of Bologna, for help in confocal microscopy experiments on Saos-2 cells, and CIRB (Centro Interdipartimentale Ricerche Biotecnologiche) of the University of Bologna for providing the Brite HS flow cytometer (BioRad, UK), the Nikon Eclipse 90i microscope equipped with a Nikon Digital Sight DS-5M telecamera, and the Nikon C1s confocal laser-scanning inverted microscope.

[1] S. J. Lippard, J. M. Berg, *Principles of Bioinorganic Chemistry*, University Science Books, Mill Valley, **1994**.
[2] W. Kaim, B. Schwederski, *Bioinorganic Chemistry: Inorganic Elements in the Chemistry of Life*, Wiley, New York, **1994**.
[3] A. Sigel, H. Sigel, R. K. O. Sigel, *Metal Ions in Life Sciences, Vol. 1: Neurodegenerative Diseases and Metal Ions*, Wiley, New York, **2006**.
[4] G. F. Nordberg, B. A. Fowler, M. Nordberg, L. Friberg, *Handbook on the Toxicology of Metals*, 3rd ed., Elsevier, Amsterdam, **2007**.
[5] E. L. Que, D. W. Domaille, C. J. Chang, *Chem. Rev.* **2008**, *108*, 1517–1549.
[6] E. M. Nolan, S. J. Lippard, *Chem. Rev.* **2008**, *108*, 3443–3480.
[7] a) G. Farruggia, S. Iotti, L. Prodi, M. Montalti, N. Zaccheroni, P. B. Savage, V. Trapani, P. Sale, F. I. Wolf, *J. Am. Chem. Soc.* **2006**, *128*, 344–350; b) G. Farruggia, S. Iotti, L. Prodi, N. Zaccheroni, M. Montalti, P. B. Savage, G. Andreani, V. Trapani, F. I. Wolf, *J. Fluoresc.* **2009**, *19*, 11–19.
[8] H. Komatsu, T. Miki, D. Citterio, T. Kubota, Y. Schindo, Y. Kitamura, K. Oka, K. Suzuki, *J. Am. Chem. Soc.* **2005**, *127*, 10798–10799.
[9] L. Zeng, E. W. Miller, A. Pralle, E. Y. Isacoff, C. J. Chang, *J. Am. Chem. Soc.* **2006**, *128*, 10–11.
[10] H. S. Jung, P. S. Kwon, J. W. Lee, J. I. Kim, C. S. Hong, J. W. Kim, S. Yan, J. Y. Lee, J. H. Lee, T. Joo, J. S. Kim, *J. Am. Chem. Soc.* **2009**, *131*, 2008–2012.
[11] E. M. Nolan, S. J. Lippard, *Acc. Chem. Res.* **2009**, *42*, 193–203.
[12] a) S. K. Ko, Y. K. Yang, J. Tae, I. Shin, *J. Am. Chem. Soc.* **2006**, *128*, 14150–14155; b) X. Guo, X. Qian, L. Jia, *J. Am. Chem. Soc.* **2004**, *126*, 2272–2273; c) Z. Zhang, X. Guo, X. Qian, Z. Liu, F. Liu, *Kidney Intern.* **2004**, *66*, 2279–2282.
[13] H. Yang, Z. Zho, K. Huang, M. Yu, F. Li, T. Yi, C. Huang, *Org. Lett.* **2007**, *9*, 4729–4732.
[14] Q. He, E. W. Miller, A. P. Wong, C. J. Chang, *J. Am. Chem. Soc.* **2006**, *128*, 9316–9317.
[15] X. Peng, J. Du, J. Wang, Y. Wu, J. Zhao, S. Sun, T. Xu, *J. Am. Chem. Soc.* **2007**, *129*, 1500–1501.
[16] T. Cheng, Y. Xu, S. Zhang, W. Zhu, X. Qian, L. Duan, *J. Am. Chem. Soc.* **2008**, *130*, 16160–16161.
[17] M. Taki, M. Desaki, A. Ojida, S. Iyoshi, T. Hirayama, I. Hamachi, Y. Yamamoto, *J. Am. Chem. Soc.* **2008**, *130*, 12564–12565.
[18] M. J. S. McLaughlin, B. R. Singh, *Cadmium in Soils and Plants*, Kluwer, Dordrecht, **1999**.

[19] S. Dobson, *Cadmium: Environmental Aspects*, World Health Organization, Geneva, **1992**.
[20] L. Friberg, C. G. Elinder, T. Kjellstřom, *Cadmium*, World Health Organization, Geneva, **1992**.
[21] T. Nawrot, M. Plusquin, J. Hogervorst, H. A. Roels, H. Celis, L. Thijs, J. Vangronsveld, E. Van Hecke, J. A. Staessen, *Lancet Oncol.* **2006**, *7*, 119–126.
[22] G. M. Cockrell, G. Zhang, D. G. VanDerveer, R. P. Thummel, R. D. Hancock, *J. Am. Chem. Soc.* **2008**, *130*, 1420–1430.
[23] C. Lu, Z. Xu, J. Cui, R. Zhang, X. Qian, *J. Org. Chem.* **2007**, *72*, 3554–3557.
[24] N. J. Williams, W. Gan, J. H. Reibenspies, R. D. Hancock, *Inorg. Chem.* **2009**, *48*, 1407–1415.
[25] a) L. Prodi, M. Montalti, N. Zaccheroni, J. S. Bradshaw, R. M. Izatt, P. B. Savage, *Tetrahedron Lett.* **2001**, *42*, 2941–2944; b) L. Prodi, *New J. Chem.* **2005**, *29*, 20–31; c) R. T. Bronson, D. J. Michaelis, R. D. Lamb, G. A. Husseini, P. B. Farnsworth, M. R. Linford, R. M. Izatt, J. S. Bradshaw, P. B. Savage, *Org. Lett.* **2005**, *7*, 1105–1108; d) M. C. Aragoni, M. Arca, A. Bencini, A. J. Blake, C. Caltagirone, G. De Filippo, F. A. Devillanova, A. Garau, T. Gelbrich, M. B. Hursthouse, F. Isaia, V. Lippolis, M. Mameli, P. Mariani, B. Valtancoli, C. Wilson, *Inorg. Chem.* **2007**, *46*, 4548–4559.
[26] a) N. Nakasuka, M. Tanaka, M. Shiro, *Acta Crystallogr. Sect. C* **1989**, *45*, 1303–1306; b) G. Serratrice, P. Baret, H. Boukholfa, I. G. Luneau, D. Luneau, J.-L. Pierr, *Inorg. Chem.* **1999**, *38*, 840–841.
[27] a) E. S. Kryachko, E. V. Ludeña, *Energy Density Functional Theory of Many Electron Systems*, Kluwer Academic Publisher, Dordrecht, **1990**; b) W. Koch, M. C. Holthausen, *A Chemist's Guide to Density Functional Theory*, 2nd ed., Wiley-VCH, Weinheim, **2002**.
[28] Selected optimized bond lengths and angles: Cd–N(1) 2.492, Cd–N(2) 2.483, Cd–S(1) 2.741, Cd–S(2) 2.743, Cd–O(1) 2.203, Cd–Ow 2.352 Å; N(1)-Cd-N(2) 95.83, N(1)-Cd-S(1) 74.61, N(1)-Cd-S(2) 75.48, N(1)-Cd-O(1) 175.22, N(1)-Cd-Ow 92.63, N(2)-Cd-S(1) 79.04, N(2)-Cd-S(2) 78.34, N(2)-Cd-O(1) 86.37, N(2)-Cd-Ow 169.10, S(1)-Cd-S(2) 140.08, S(1)-Cd-O(1) 101.72, S(1)-Cd-Ow 109.94, S(2)-Cd-O(1) 109.16, S(2)-Cd-Ow 97.23, O(1)-Cd-Ow 85.72°; angle between the plane containing the 5-Cl-8HDQ moiety and the pseudoplane defined by the metal center and the N(1), N(2), O(1), and Ow atoms: 27.20°.
[29] a) A. E. Reed, F. Weinhold, *J. Chem. Phys.* **1983**, *78*, 4066–4073; b) A. E. Reed, R. B. Weinstock, F. Weinhold, *J. Chem. Phys.* **1985**, *83*, 735–746; c) A. E. Reed, L. A. Curtiss, F. Weinhold, *Chem. Rev.* **1988**, *88*, 899–926.
[30] K. Wiberg, *Tetrahedron* **1968**, *24*, 1083–1096.
[31] K. Andersson, P.-A. Malmqvist, B. O. Roos, A. J. Sadlej, K. Wolinski, *J. Phys. Chem.* **1990**, *94*, 5483–5488.
[32] H. Nakatsuji, *Chem. Phys. Lett.* **1978**, *59*, 362–364.
[33] See, for example, a) F. Mendizabal, B. Aguilera, C. Olea-Azar, *Chem. Phys. Lett.* **2007**, *447*, 345–351; b) C. J. Adams, N. Fey, Z. A. Harrison, I. V. Sazanovich, M. Towrie, J. A. Weinstein, *Inorg. Chem.* **2008**, *47*, 8242–8257; c) A. Díez, J. Forniés, S. Fuertes, E. Lalinde, C. Larraz, J. A. López, A. Martín, M. T. Moreno, V. Sicilia, *Organometallics* **2009**, *28*, 1705–1718.
[34] a) H. Xu, L.-F. Huang, L.-M. Guo, Y.-G. Zhang, X.-M. Ren, Y. Song, J. Xie, *J. Lumin.* **2008**, *128*, 1665–1669; b) S. Salehzadeh, R. Golbedaghi, I. S. Tidmarsh, N. K. Al-Rasbi, H. Adams, M. D. Ward, *Polyhedron* **2008**, *27*, 3549–3556.
[35] a) A. D. Becke, *J. Chem. Phys.* **1993**, *98*, 5648–5652; b) C. Lee, W. Yang, R. G. Parr, *Phys. Rev. B* **1988**, *37*, 785–789.
[36] A. Schäfer, H. Horn, R. J. Ahlrichs, *Chem. Phys.* **1992**, *159–168*, 2571–2577.
[37] a) T. H. Dunning, Jr., P. J. Hay in *Methods of Electronic Structure, Theory, Vol. 2*, 3rd ed. (Ed.: H. F. Schaefer), Plenum Press, New York, **1977**; b) J. V. Ortiz, P. J. Hay, R. L. Martin, *J. Am. Chem. Soc.* **1992**, *114*, 2736–2737.
[38] a) M. Goldman, E. L. Wehry, *Anal. Chem.* **1970**, *42*, 1178–1185; b) S. G. Schulman, *Anal. Chem.* **1971**, *43*, 285–287.
[39] a) M. R. Nimlos, D. F. Kelley, E. R. Bernstein, *J. Phys. Chem.* **1987**, *91*, 6610–6614; b) E. Bardez, I. Devol, B. Larrey, B. Valeur, *J. Phys. Chem. B* **1997**, *101*, 7786–7793; c) L. Prodi, C. Bargossi, M. Montalti, N. Zaccheroni, N. Su, J. S. Bradshaw, R. M. Izatt, P. B. Savage, *J. Am. Chem. Soc.* **2000**, *122*, 6769–6770; d) L. Prodi, M. Montalti, J. S. Bradshaw, R. M. Izatt, P. B. Savage, *J. Inclusion Phenom. Macrocyclic Chem.* **2001**, *41*, 123–127; e) R. T. Bronson, M. Montalti, L. Prodi, N. Zaccheroni, R. D. Lamb, N. K. Dalley, R. M. Izatt, J. S. Bradshaw, P. B. Savage, *Tetrahedron Lett.* **2004**, *45*, 11139–11144.
[40] P. Gans, A. Sabatini, A. Vacca, *Talanta* **1996**, *43*, 1739–1753.
[41] P. Pallavicini, Y. A. Diaz-Fernandez, L. Pasotti, *Coord. Chem. Rev.* **2009**, *253*, 2226–2240.
[42] R. De Paula, A. E. da Hora Machado, J. A. de Miranda, *J. Photochem. Photobiol. A* **2004**, *165*, 109–114.
[43] E. Fuguet, C. Ràfols, M. Rosés, E. Bosch, *Anal. Chim. Acta* **2005**, *548*, 95–100.
[44] a) H. Gampp, M. Maeder, C. J. Mayer, A. D. Zuberbühler, *Talanta* **1985**, *32*, 95–101; b) H. Gampp, M. Maeder, C. J. Mayer, A. D. Zuberbühler, *Talanta* **1985**, *32*, 251–264; c) M. Maeder, A. D. Zuberbühler, *Anal. Chem.* **1990**, *62*, 2220–2224.
[45] C. S. Johnson, Jr., *Prog. Nucl. Magn. Reson. Spectrosc.* **1999**, *34*, 203–256.
[46] A. Sacco, E. Matteoli, *J. Solution Chem.* **1997**, *26*, 527–535.
[47] D. Beyersmann, H. Haase, *Biometals* **2001**, *14*, 331–341.
[48] a) K. G. Coonse, A. J. Coonts, E. V. Morrison, S. J. Heggland, *J. Toxicol. Environ. Health Part A* **2007**, *70*, 575–581; b) D. Bagchi, S. S. Joshi, M. Bagchi, J. Balmoori, E. J. Benner, C. A. Kuszynksi, S. J. Stohs, *J. Biochem. Mol. Toxicol.* **2000**, *14*, 33–41.
[49] A. D. Bangham, M. M. Stondish, J. C. Watkins, *J. Mol. Biol.* **1965**, *13*, 238–252.
[50] SADABS, Area-Detector Absorption Correction Program, Bruker AXS, Inc., Madison, WI, **2003**.
[51] A. Altomare, M. C. Burla, M. Camalli, G. Cascarano, C. Giacovazzo, A. Gagliardi, G. Polidori, *J. Appl. Crystallogr.* **1994**, *27*, 435–436.
[52] SHELXL 97: G. M. Sheldrick, *Acta Crystallogr. Sect. A* **2008**, *64*, 112–122.
[53] a) A. Credi, L. Prodi, *Spectrochim. Acta* **1998**, *54*, 159–170; b) M. Montalti, A. Credi, L. Prodi, M. T. Gandolfi, *Handbook of Photochemistry*, 3rd ed., Taylor & Francis, Boca Raton, **2006**.
[54] L. Yang, R. McRae, M. M. Henary, R. Patel, B. Lai, S. Vogt, C. J. Fahrni, *Proc. Natl. Acad. Sci. USA* **2005**, *102*, 11179–11184.
[55] Gaussian 03, Revision E1, M. J. Frisch, G. W. Trucks, H. B. Schlegel, G. E. Scuseria, M. A. Robb, J. R. Cheeseman, J. A. Montgomery, Jr., T. Vreven, K. N. Kudin, J. C. Burant, J. M. Millam, S. S. Iyengar, J. Tomasi, V. Barone, B. Mennucci, M. Cossi, G. Scalmani, N. Rega, G. A. Petersson, H. Nakatsuji, M. Hada, M. Ehara, K. Toyota, R. Fukuda, J. Hasegawa, M. Ishida, T. Nakajima, Y. Honda, O. Kitao, H. Nakai, M. Klene, X. Li, J. E. Knox, H. P. Hratchian, J. B. Cross, V. Bakken, C. Adamo, J. Jaramillo, R. Gomperts, R. E. Stratmann, O. Yazyev, A. J. Austin, R. Cammi, C. Pomelli, J. W. Ochterski, P. Y. Ayala, K. Morokuma, G. A. Voth, P. Salvador, J. J. Dannenberg, V. G. Zakrzewski, S. Dapprich, A. D. Daniels, M. C. Strain, O. Farkas, D. K. Malick, A. D. Rabuck, K. Raghavachari, J. B. Foresman, J. V. Ortiz, Q. Cui, A. G. Baboul, S. Clifford, J. Cioslowski, B. B. Stefanov, G. Liu, A. Liashenko, P. Piskorz, I. Komaromi, R. L. Martin, D. J. Fox, T. Keith, M. A. Al-Laham, C. Y. Peng, A. Nanayakkara, M. Challacombe, W. P. M. Gill, B. Johnson, W. Chen, M. W. Wong, C. Gonzalez, J. A. Pople, Gaussian, Inc., Wallingford, CT, **2004**.
[56] Basis sets were obtained from the Extensible Computational Chemistry Environment Basis Set Database.
[57] a) D. J. Feller, *Comput. Chem.* **1996**, *17*, 1571–1586; b) K. L. Schuchardt, B. T. Didier, T. Elsethagen, L. Sun, V. Gurumoorthi, J. Chase, J. Li, T. L. Windus, *J. Chem. Inf. Model.* **2007**, *47*, 1045–1052.
[58] G. Schaftenaar, J. H. Noordik, *J. Comput.-Aided Mol. Des.* **2000**, *14*, 123–134.

Received: July 20, 2009
Published online: November 26, 2009

